Supporting Information

The Influence of Structure and Processing on the Behavior of TiO_2 Protective Layers for Stabilization of n-Si/TiO_2/Ni Photoanodes for Water Oxidation

Matthew T. McDowell[1,2], Michael F. Lichterman[1,2], Azhar I. Carim[1], Rui Liu[1,2], Shu Hu[1,2], Bruce S. Brunschwig[2,3], Nathan S. Lewis*[1,2,3,4]

[1]Division of Chemistry and Chemical Engineering, 210 Noyes Laboratory, California Institute of Technology, Pasadena, CA, 91125, USA
[2]Joint Center for Artificial Photosynthesis, California Institute of Technology, 1200 E. California Blvd., Pasadena, CA, 91125, USA
[3]Beckman Institute, California Institute of Technology, Pasadena, CA, 91125, USA
[4]Kavli Nanoscience Institute, California Institute of Technology, Pasadena, CA, 91125, USA

**Corresponding author, nslewis@caltech.edu*

I. Detailed Experimental Methods

A. RCA cleaning of Si. To fabricate electrodes, n-Si (ρ = 0.5 Ω-cm) or p^+-Si (ρ = 0.005 Ω-cm) wafers with (111) orientation were first cleaved into pieces, and these pieces were RCA cleaned. RCA cleaning consisted of i) soaking in a 5:1:1 $H_2O/H_2O_2/NH_4OH$ solution at 75°C for 10 min, ii) etching the native oxide from the wafers with 10 vol % HF, and then iii) soaking in a 5:1:1 H_2O/H_2O_2/HCl solution at 75°C for 10 min. The wafers were then thoroughly rinsed with distilled, deionized H_2O (Millipore, resistivity of 18.2 MΩ·cm) and dried with nitrogen before immediately being inserted into either an ALD chamber or sputterer for TiO_2 deposition.

B. ALD of TiO_2. ALD was performed with two different processes involving different Ti precursors. The films grown using TDMAT (tetrakis-dimethylamidotitanium, Sigma-Aldrich, 99.999%) were deposited in a Cambridge Nanotech S200 ALD system. Each ALD cycle consisted of a 0.015 s pulse of distilled, deionized H_2O, followed by a 0.10 s TDMAT pulse. After each pulse, N_2(g) was purged within the chamber for 15 s at a flow rate of 20 sccm. The substrate was maintained at 150°C during the deposition, and the TDMAT precursor was heated to 75°C with a heating jacket. The H_2O was maintained at room temperature. For films grown using TTIP (titanium tetraisopropoxide, Strem Chemicals, 98%), a Cambridge Nanotech Fiji F200 ALD system was used. Each ALD cycle consisted of a 0.2 s pulse of TTIP, followed by a 0.06 s pulse of distilled, deionized H_2O. After each pulse, Ar(g) was purged within the chamber for 5 s at a flow rate of 260 sccm. The substrate was maintained at 250°C during deposition, and the TTIP precursor was heated to 75°C.

C. Annealing of samples. Some TDMAT-ALD samples were annealed in either air or forming gas environments after deposition of TiO_2. Samples were heated to temperatures between 400 and 775°C for 40-60 min. Air-annealed samples were heated in a muffle furnace (Thermo Scientific Thermolyne), and forming-annealed samples were heated in a tube furnace (Mellen). Forming gas (5% H_2, 95% N_2) was flowed at 4-5 LPM into the ½ inch quartz tube that held the sample and was vented through a narrow copper tube at the other end.

D. Sputtering of TiO_2. An AJA Orion sputtering system was used for all sputter depositions. TiO_2 was sputtered using a DC power source and a Ti metal target (ACI Alloys, 99.95%) in an Ar/O_2 plasma. A power of 200 W and gas flow rates of 16 sccm Ar and 1 sccm O_2 were used. The chamber was maintained at a pressure of 5 mTorr during deposition. The sample was heated to a temperature of 400°C during deposition.

E. Sputtering of Ni. After TiO_2 was deposited and in some cases annealed, a thin (~5 nm) Ni layer was sputtered onto cleaved wafer pieces to form the final thin film stacks. Wafer pieces with areas of 0.05-0.1

cm^2 were masked around the edges with Kapton tape to avoid Ni deposition onto bare Si, and they were inserted into the sputtering system. Ni (ACI Alloys, 99.95%) was sputtered with an RF power source set to 150 W, an Ar flow rate of 17 sccm, and an Ar pressure of 8.5 mTorr. The sputtering time was 4 min.

F. X-ray diffraction. XRD was performed on a Bruker DISCOVER D8 instrument with Cu Kα radiation. The background was subtracted from the XRD scans with Bruker DIFFRAC.EVA software. TiO_2 films on amorphous substrates (glass or fused quartz (Chemglass)) were used to avoid the strong diffraction peaks that would be generated by Si.

G. Raman spectroscopy. TiO_2 samples for Raman spectroscopy consisted of TiO_2 deposited on Ti metal substrates. Raman spectra were collected with a Renishaw inVia Raman microprobe equipped with a Leica DM 2500 M microscope, a Leica N Plan 50x objective (numerical aperture = 0.75), a 1800 lines mm^{-1} grating, and a CCD detector configured in a 180° backscatter geometry. A 532 nm diode-pumped solid-state (DPSS) laser (Renishaw RL532C50) was used as the excitation source and a 23.5 mW radiant flux was incident on the surface of the sample. A line-focus lens was utilized to transform the circular incident beam in one dimension to generate a ca. 50 μm line at the sample. A λ/4 plate was used to circularly polarize the incident excitation. No polarizing collection optic was used.

H. X-ray photoelectron spectroscopy. XPS was performed in separate experiments to collect spectra from the Ti core levels as well as the valence-band energy region. All XPS samples consisted of TiO_2 deposited on p^+-Si. Core-level spectra were acquired using a Surface Science Instruments M-Probe instrument with Al Kα x-rays, a hemispherical energy analyzer, and a takeoff angle of 35 degrees. The Ti2p peaks were corrected for the position of the C1s peak in the spectrum (prescribed to be at 285.0 eV), and they were fitted with a Shirley background. Valence spectra were collected on a Kratos AXIS Ultra system with a base pressure of $<2\times10^{-9}$ Torr. A monochromatic Al Kα source was used to irradiate the sample with X-rays with an energy of 1486.7 eV at a power of 150 W. A hemispherical analyzer oriented for detection along the sample surface normal was used for maximum depth sensitivity. High-resolution spectra were acquired at a resolution of 50 meV with a pass energy of 20 eV.

I. Transmission electron microscopy. Cross-sectional TEM samples were made with conventional polishing and milling techniques. $Si/TiO_2/Ni$ samples were first cleaved into ~5 mm by ~2 cm strips, and two pieces were glued face-to-face with M-Bond 610 adhesive. These pieces were then cut with a diamond saw into ~1 mm thick cross-section samples, which were polished on one side and then glued to Mo TEM slot grids (SPI Supplies) with M-Bond. The samples were then manually polished first with sand paper and then with progressively finer diamond lapping film discs (Allied High Tech Products, Inc.) until the cross sections were ~20 μm thick. The samples were then placed on a dimpler (E.A.

Fischione Instruments, Inc., Model 2000), where they were further polished before the final step of ion milling with Ar ions until the samples were of appropriate thickness for TEM imaging. An FEI Tecnai F30ST microscope with an accelerating voltage of 300 kV was used for imaging.

J. Four-point probe measurements. Four-point probe measurements were carried out on 100 nm thick TiO_2 films deposited onto fused quartz substrates. Indium metal was soldered at four locations on the surface of the TiO_2 to ensure ohmic contact. A Jandel four-point probe device, in combination with a custom Labview program, was used for measurement.

K. Impedance spectroscopy. Impedance spectroscopy was performed in the solid state on p^+-Si/TiO_2/Ni devices. Electrical contact was made to the p^+-Si with In-Ga alloy coated with Ag paint, and electrical contact was made to the Ni with Ag paint. A Bio-logic SP-200 potentiostat was used, and impedance spectroscopy was performed at a bias of 0 V by sweeping between 1 MHz and 10 Hz and using a sine-wave amplitude of 5.0 mV.

L. Secondary ion mass spectrometry (SIMS). SIMS depth-profiling analysis was performed with a Cameca IMS 7f-GEO instrument. The TiO_2 films were deposited on p^+-Si substrates for SIMS analysis. A Cs^+ ion beam was used to ionize and sputter surface atoms from each of the TiO_2 thin films. The ion beam current utilized was ~7 nA, and the raster area was ~50 μm^2. Count rates from ^{28}Si, ^{12}C, ^{18}O, and $^{14}N+^{12}C$ (a complex ion) were detected as a function of sputtering time.

II. Supplemental Data

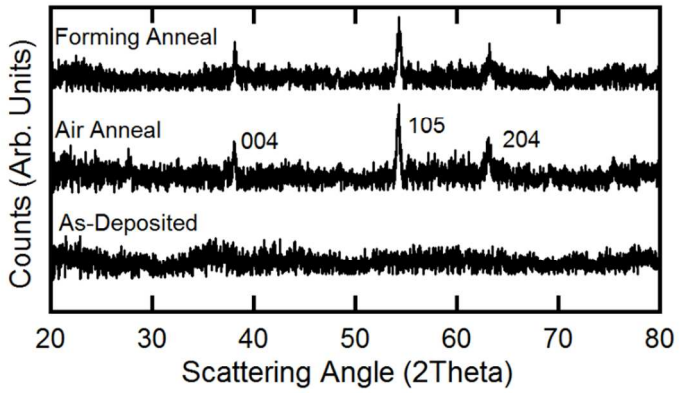

Figure S1. X-ray diffraction of ~100 nm thick as-deposited and annealed TDMAT-ALD films on fused quartz. The annealed films were heated to 450 °C for 1 h. The as-deposited film is amorphous, while the annealed films show anatase peaks. Not all the anatase peaks are visible, presumably because of preferential orientation of the crystals in the film.

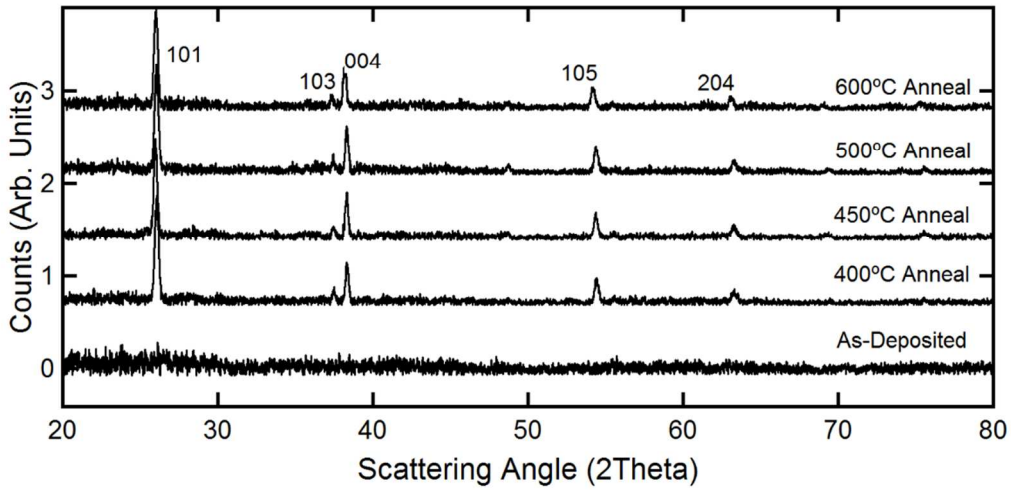

Figure S2. X-ray diffraction of ~100 nm thick as-deposited TDMAT-ALD films and films annealed at different temperatures in air. All films annealed between 400 °C and 600 °C convert to the anatase phase, as shown by the labeled diffraction peaks. Annealing at 600 °C also produces a minority rutile phase, which is not evident from X-ray diffraction but is detected by Raman spectroscopy (Fig. S8).

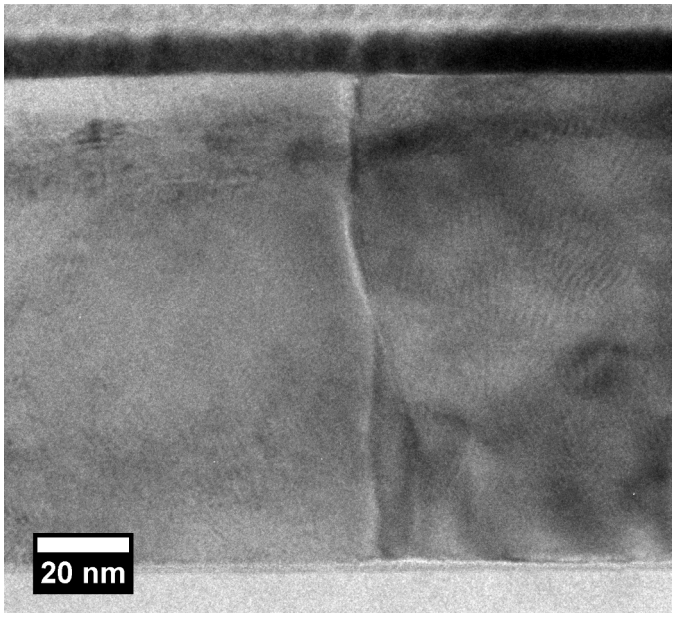

Figure S3. Low-magnification cross-sectional TEM image of a TDMAT-ALD film annealed at 500 °C in air. The image shows a vertical grain boundary between two crystals in the film. The Si substrate is at the bottom of the image, and a Ni layer is visible at the top.

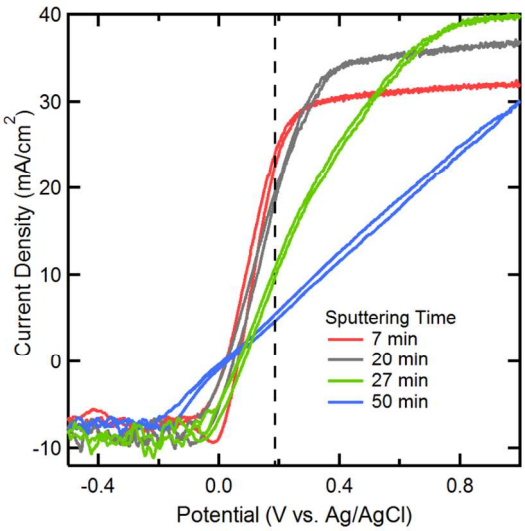

Figure S4. Current-potential curves of n-Si/TiO_2/Ni electrodes with sputtered TiO_2 of varying thickness under 1-sun illumination in 0.35 M $K_4Fe(CN)_6$/0.050 M $K_3Fe(CN)_6$ aqueous electrolyte. As the TiO_2 thickness increases from ~25 nm (7 min sputtering time) to ~180 nm (50 min sputtering time), the *J-E* curves become more resistive. This contrasts with the *J-E* thickness dependence of samples with as-deposited TDMAT-ALD, which exhibit similar *J-E* characteristics between ~4 and ~150 nm in thickness. The vertical dashed line denotes the Nernstian potential of the electrolyte. These data show that the film thickness for different types of TiO_2 must be tuned independently for optimal performance.

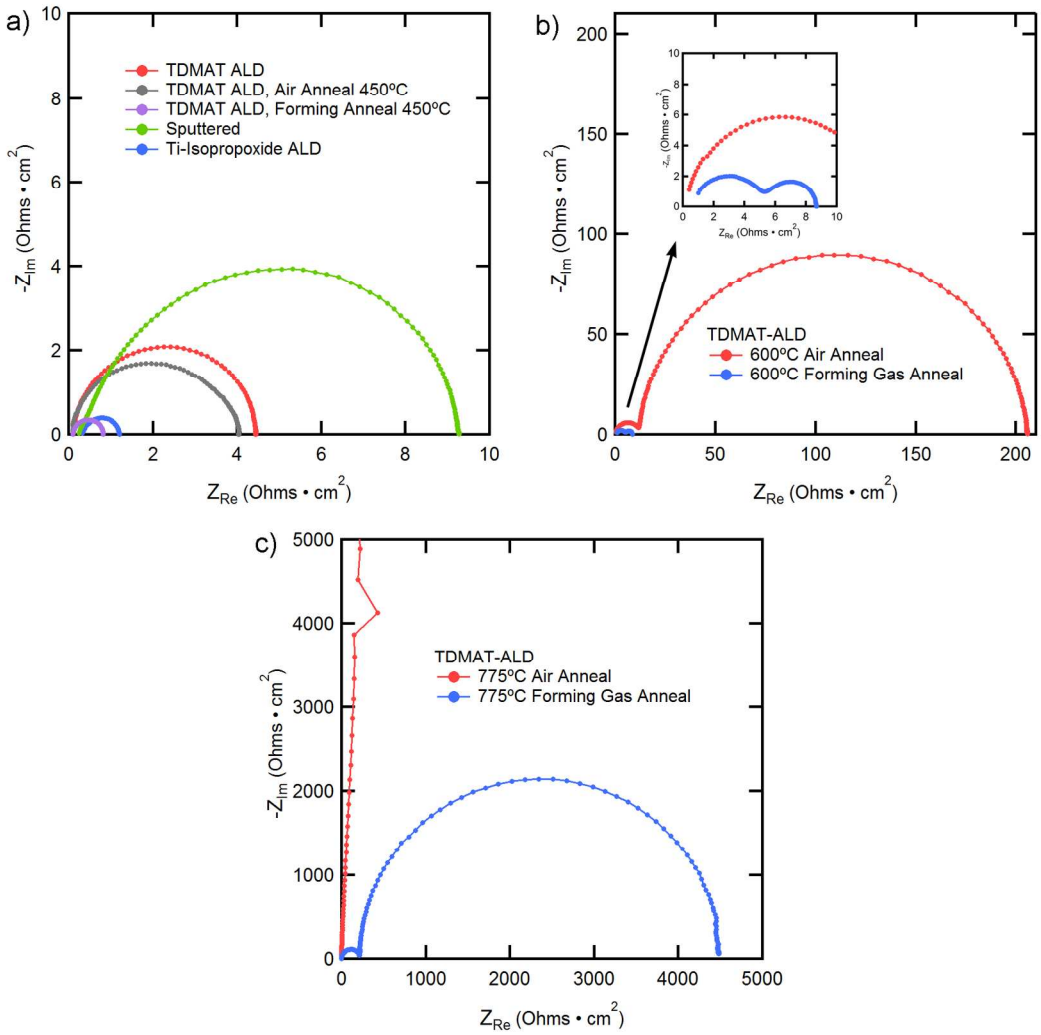

Figure S5. Impedance spectroscopy of p^+-Si/TiO_2/Ni solid-state devices with ~100 nm thick TiO_2 layers. Each of the devices was tested with an In-Ga back contact and a Ni front contact. a) Impedance spectra from devices containing TiO_2 that was deposited or processed at $T < 500$ °C. The Nyquist plot revealed a single depressed semicircle for all of the samples, indicating that the TiO_2 layers alone controlled the impedance response. The diameter of the semicircle was the largest for the sputtered sample, indicating the highest resistance, which matches the electrochemical data shown in Fig. S4. In addition, the semicircle from the sputtered sample was slightly distorted, which may arise from the high density of columnar grain boundaries in the sputtered film. b) Impedance spectra from TDMAT-ALD samples annealed at 600 °C in either forming gas or air. The inset shows a magnified view of the low-Z region. The spectrum for each of the samples consisted of two overlapping semicircles, suggesting the growth of an interfacial SiO_x film. Both semicircles from the air-annealed sample had greater diameters than those exhibited by the forming-annealed sample, indicating that the resistance of both the SiO_x at the interface and the TiO_2 are greater in the air-annealed sample than in the forming-gas-annealed sample. c) Impedance spectra from TDMAT-ALD samples annealed at 775 °C in forming gas or in air.

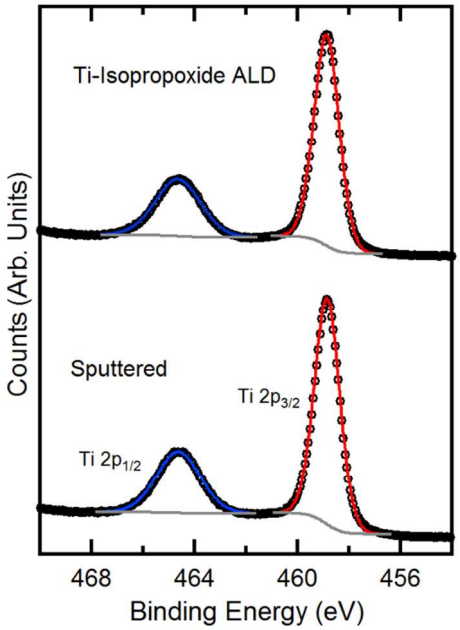

Figure S6. Ti 2p XPS peaks for sputtered and TTIP-ALD films. XPS depth profiling was not performed because the harsh nature of sputtering can change the oxidation state or chemical environment of species within a material.

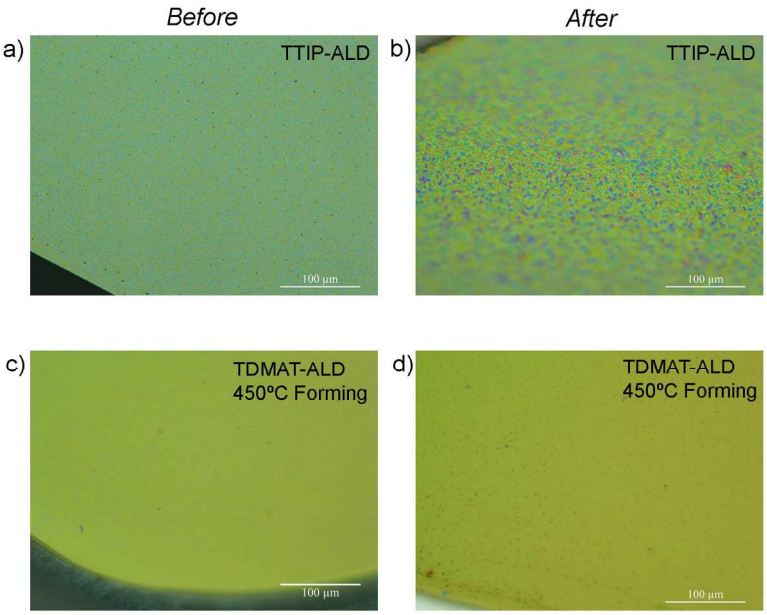

Figure S7. Optical microscopy images of the surface of n-Si/TiO_2/Ni electrodes with two different types of TiO_2 before and after chronoamperometry in 1.0 M KOH(aq) under illumination. a-b) TTIP-ALD films before and after 60 h of operation. The surface of the film after the chronoamperometry was noticeably pockmarked and damaged. c-d) TDMAT-ALD films annealed in forming gas at 450 °C before and after 100 h of operation. The surface of the sample after testing (d) was smoother and exhibited less obvious damage than the TTIP-ALD material, in accord with the observed photocurrent stability of the TDMAT-ALD films.

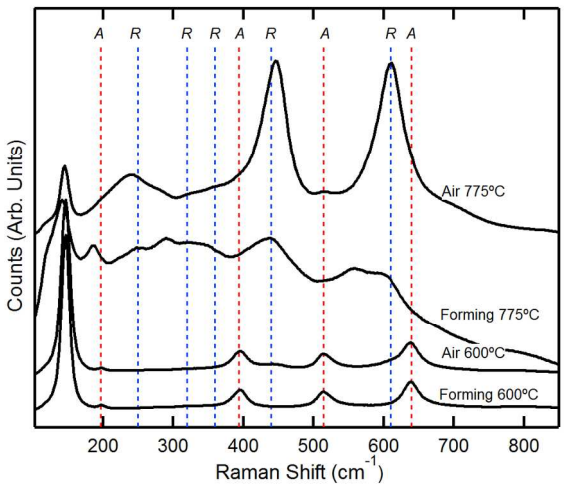

Figure S8. Raman spectra of TiO_2 films annealed at higher temperatures (600 °C and 775 °C) in air and forming gas. The *R* and *A* labels correspond to the various modes of the rutile (*R*) and anatase (*A*) phases. The 600 °C films are primarily anatase, with a minor rutile component in the air-annealed sample. The 775 °C films are rutile with minor anatase components.

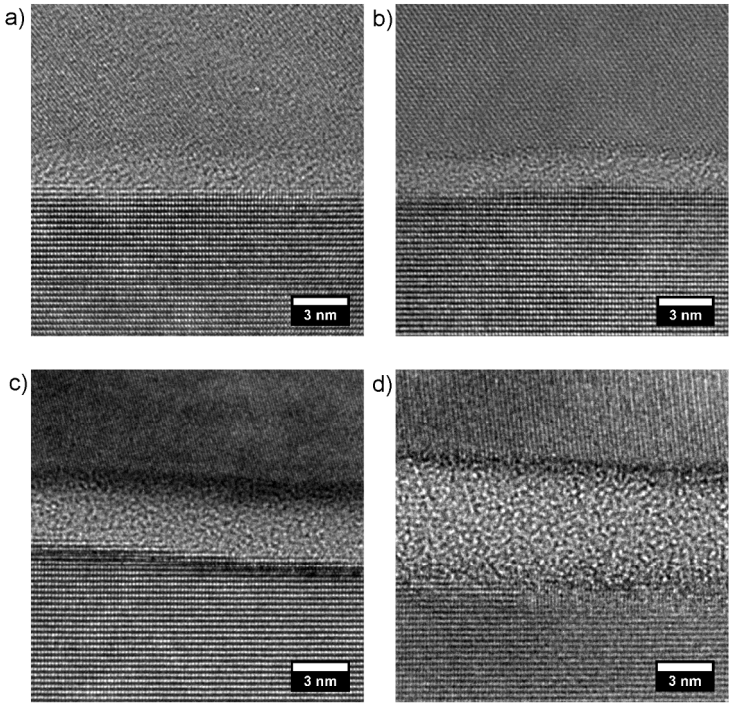

Figure S9. High-resolution cross-sectional TEM images of the Si/TiO_2 interface from TDMAT-ALD TiO_2 samples annealed at higher temperatures (600 and 775 °C) in air or forming gas for 1 h. The Si lattice is at the bottom of the images, and the TiO_2 is at the top. The interfacial SiO_x layer is amorphous. a) 600 °C anneal in forming gas; b) 600 °C anneal in air; c) 775 °C anneal in forming gas; d) 775 °C anneal in air. Note that average SiO_x thicknesses calculated from TEM images are tabulated in Table 1 in the main text.

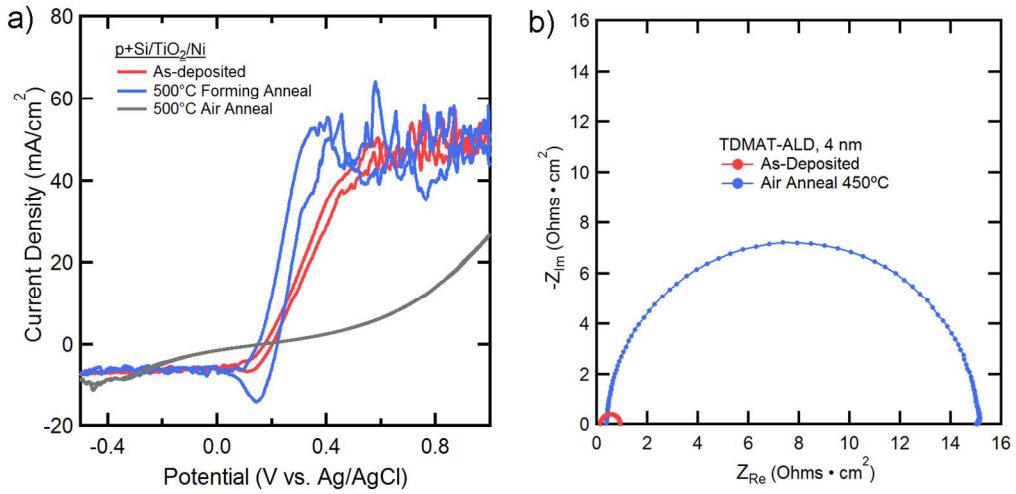

Figure S10. a) Dark *J-E* behavior of p^+-Si/TiO_2/Ni electrodes with thin (4 nm) TiO_2 layers in contact with 0.35 M $K_4Fe(CN)_6$/0.050 M $K_3Fe(CN)_6$(aq). The samples with as-deposited and forming-gas-annealed TiO_2 were highly conductive, while the air-annealed sample showed reduced conductivity. This behavior is in contrast to the samples with thicker (~100 nm) TiO_2 films discussed in the main text. Note that the current fluctuations in the high-potential region are due to diffusion limitation of the redox species in the stirred electrolyte. b) Impedance spectra of solid-state devices with 4 nm TiO_2 layers. Both the as-deposited TiO_2 device and the device with annealed TiO_2 exhibited single semicircles, indicating negligible growth of a SiO_x interfacial layer.

III. SIMS Analysis

To detect the presence of carbon and nitrogen impurities in the films, SIMS depth profiling was performed on the set of five TiO_2 films that were annealed or deposited at moderate temperatures. Figure S11 shows the carbon, nitrogen, oxygen, and silicon signals observed through the thickness of an as-deposited TDMAT-ALD film. This film was ~105 nm thick, which corresponds to ~60 sputter steps on the x-axis of the plot. The silicon signal increased and the carbon, nitrogen, and oxygen signals decreased to a baseline level after entirely sputtering through the TiO_2 film. Fig. S11 indicates the presence of carbon and nitrogen impurities throughout the TiO_2 film, in accord with previous results (S. Hu *et al., Science,* (2014), 344, 6187, 1005-1009). These data do not represent absolute concentrations, because the detected counts depend on a number of factors, including the sputtering yield and the relative abundance of each selected isotope.

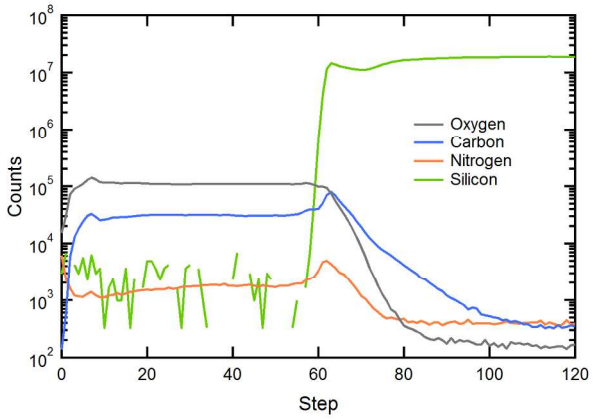

Figure S11. SIMS depth profile from an as-deposited TDMAT-ALD film. The fluctuations of the silicon signal on the left side of the plot arise because of the low concentration of silicon in this region (a Faraday cup was used for silicon detection).

Comparison of the relative carbon and nitrogen counts among the different TiO_2 films yields useful information regarding the carbon and nitrogen content in the films. Because the total oxygen content in all the TiO_2 films is expected to be similar, the ^{12}C:^{18}O and the (^{14}N+^{12}C):^{18}O ratios were calculated through the thickness of each film to provide a comparison of the relative content of carbon and nitrogen, respectively. Such plots of the relative carbon and nitrogen signals from films that were fabricated or annealed at moderate temperatures ($\leq$ 500 °C) are shown in Fig. S12. Figure S12a shows that all of these films contained carbon impurities. The TDMAT-ALD films (both as-deposited and annealed in air/forming gas) contained a constant and mutually similar amount of carbon through the thickness of the films. The sputtered film contained more carbon, while the TTIP-ALD films contained less carbon than the TDMAT-ALD films. In addition, the carbon signals varied with depth in these films. The detected nitrogen signals (Fig. S12b) showed a similar trend, with the TDMAT-ALD films exhibiting similar nitrogen content and with more nitrogen in the sputtered film and less nitrogen in the TTIP-ALD film than in the TDMAT-ALD films. The nitrogen signal in the TTIP-ALD film increased near the Si/TiO_2 interface. Taken together, these results indicate that all these films contained carbon and nitrogen with different concentrations. Furthermore, the mutually similar content of carbon and nitrogen in the as-deposited and annealed TDMAT-ALD films suggests that the changes in the mid-gap states (Fig. 6 in the main text) observed after annealing are not primarily due to changes in impurity content.

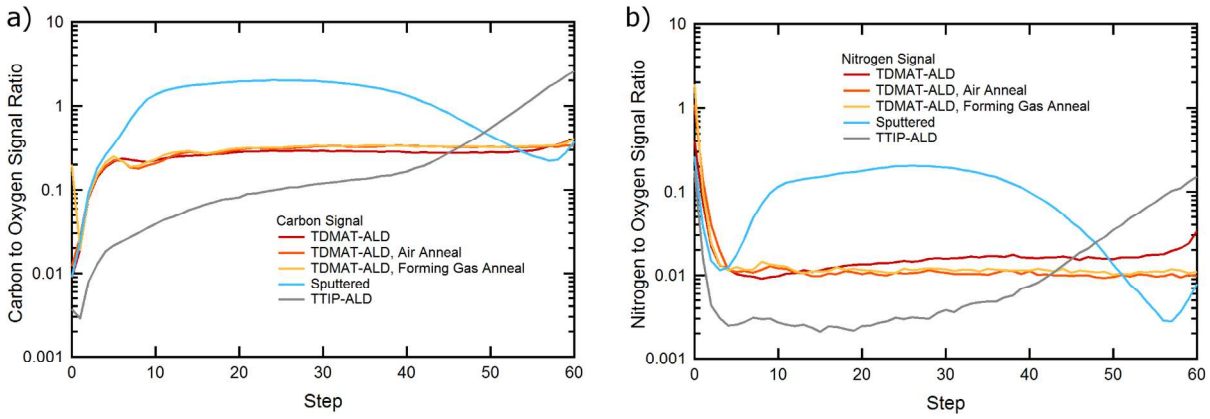

Figure S12. SIMS data showing the carbon-to-oxygen signal ratio (a) and the nitrogen-to-oxygen signal ratio (b) through the thickness of five different ~100 nm thick TiO_2 films (these are films deposited or processed at temperatures ≤ 500 °C). In (a), the ^{12}C:^{18}O ratio is displayed, and in (b), the (^{14}N+^{12}C):^{18}O ratio is displayed. The left side of these plots (step 0) corresponds to the surface of the films, and the right side (step 60) corresponds to the Si/TiO_2 interface. The annealed films were annealed at 450 °C.

Figure S13 shows similar data for TDMAT-ALD films that were annealed at higher temperatures (600 and 775 °C) compared to an as-deposited film from the same batch. Both the carbon-to-oxygen ratio (^{12}C:^{18}O) and the nitrogen-to-oxygen ratio ((^{14}N+^{12}C):^{18}O) are shown in this plot. The carbon signals (solid lines) of the as-deposited film and the annealed films were mutually similar, indicating that the films had similar carbon contents. The nitrogen signals (dotted lines) of the annealed films varied in magnitude, and the films annealed at 600 and 775 °C in air, as well as the film annealed at 600 °C in forming gas, had slightly higher nitrogen content than the as-deposited film, while the film annealed at 775 °C in forming gas had a lower nitrogen content.

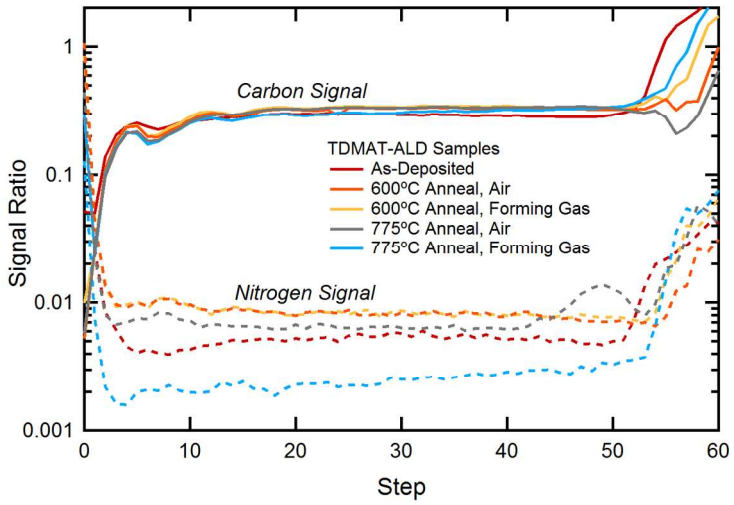

Figure S13. SIMS data showing the ^{12}C:^{18}O ratio and the (^{14}N+^{12}C):^{18}O ratio over the thickness of an as-deposited TDMAT-ALD film and TDMAT-ALD films annealed at higher temperatures (600 °C and 775

°C) in air or in forming gas. Solid lines represent the carbon signals, while dashed lines represent the nitrogen signals.